REDUCED RISK OF NORTH AMERICAN COLD EXTREMES DUE TO CONTINUED ARCTIC SEA ICE LOSS

BY JAMES A. SCREEN[1*], CLARA DESER[2] AND LANTAO SUN[2]

[1]College of Engineering, Mathematics and Physical Sciences, University of Exeter, Exeter, Devon, EX4 4QE, UK

[2]Climate and Global Dynamics, National Center for Atmospheric Research, Boulder, Colorado, 80307, US

*Corresponding author: j.screen@exeter.ac.uk

ABSTRACT

In early-January 2014, an Arctic air outbreak brought extreme cold and heavy snowfall to central and eastern North America, causing widespread disruption and monetary losses. The media extensively reported the cold snap, including debate on whether or not human-induced climate change was partly responsible. Related to this, one particular hypothesis garnered considerable attention: that rapid Arctic sea ice loss may be increasing the risk of cold extremes in mid-latitudes. Here we use large ensembles of model simulations to explore how the risk of North American daily cold extremes is anticipated to change in the future, in response to increases in greenhouse gases and the component of that response due solely to Arctic sea ice loss. Specifically, we examine the changing probability of daily cold extremes as (un)common as the 7 January 2014 event. Projected increases in greenhouse gases decrease the likelihood of North American cold extremes in the future. Days as cold or colder than the 7 January 2014 are still projected to occur in the mid twenty-first century (2030-49), albeit less frequently than in the late twentieth century (1980-99). However, such events will cease to occur by the late twenty-first century (2080-99), assuming greenhouse gas emissions continue unabated. Continued Arctic sea ice loss is a major driver of decreased - not increased - North America cold extremes. Projected Arctic sea ice loss alone reduces the odds of such an event by one quarter to one third by the mid twenty-first century, and to zero (or near-zero) by the late twenty-first century.

CAPSULE

North American cold extremes are expected to become less frequent as a result of continued Arctic sea ice loss, contrary to recent claims

INTRODUCTION

In early-January 2014, an Arctic air outbreak brought extreme cold to central and eastern North America. Record low minimum temperatures for the calendar date were set at many weather stations, including at Chicago (O'Hare Airport, -26.7°C/-16°F, 6 Jan), New York (Central Park, -15.6°C/4°F, 7 Jan), Washington DC (Dulles Airport, -17.2°C/1°F, 7 Jan), and as far south as Atlanta (-14.4°C/6°F, 7 Jan) and Austin (Bergstrom Airport, -11.1°C/12°F, 7 Jan)[1]. Daily maximum snowfall records were also broken at several stations, including Buffalo (7.6", 8 Jan) and St Louis (10.8", 5 Jan).

The cold temperatures and heavy snowfall caused widespread disruption to transport and power supply, closure of work places and public services, and damage to agricultural crops; all with significant economic implications. Unsurprisingly given the disruption, the national and global media extensively reported the cold snap, including debate on whether or not human-induced climate change was partly responsible. Related to this, one particular hypothesis garnered considerable attention: the suggestion that rapid Arctic warming and associated sea ice loss may be increasing the risk of cold extremes.

[1] Data from the National Weather Service (http://www.nws.noaa.gov/climate)

The media were not alone in making this link. In the midst of the frigid conditions, the White House released a public information video claiming that, paradoxically, cold extremes will become more likely as a result of global warming. President Obama's Science Advisor, Dr John Holdren, stated:

"…the kind of extreme cold being experienced by much of the United States as we speak is a pattern that we can expect to see with increasing frequency as global warming continues."

The cited explanation was that Arctic sea ice loss specifically, or Arctic amplification (the greater warming of the Arctic than lower latitudes) more generally, is increasing the likelihood of the type of weather patterns that lead to cold extremes. The scientific basis for this statement is derived from a number of recent observational and modeling studies (Honda et al., 2009; Petoukhov and Semenov, 2010; Francis and Vavrus, 2012; Inoue et al., 2012; Liu et al., 2012; Yang and Christensen, 2012; Tang et al., 2013; Cohen et al., 2014; Vihma, 2014; Walsh, 2014).

However, key aspects of some of these aforementioned studies have been questioned (Barnes 2013; Screen and Simmonds, 2013; Barnes et al., 2014; Gerber et al., 2014; Woolings et al., 2014) and counter arguments put forward (Hassanzadeh et al., 2014; Fischer and Knutti, 2014; Screen, 2014; Wallace et al., 2014). Furthermore, these studies have largely focused on relationships in the present-day climate. Only a few studies have considered the global impacts of future sea ice loss (e.g., Deser et al., 2010; Peings and Magnusdottir, 2014; Deser et al, 2014) and these have focused on seasonal-mean changes. Future changes in cold extremes in response to projected Arctic sea ice loss require further study. Here we specifically focus on North America, prompted by the events of the past winter and the extensive media coverage it received.

HOW UNUSUAL WAS WINTER 2013/14?

We start with a brief overview of the winter of 2013/14, based on gridded temperature data from the NCEP-NCAR reanalysis (Kalnay et al., 1996). The period December 2013 through February 2014 was, on average, anomalously cold over most of North America east of the Rocky Mountains (Fig. 1a), while the Southwest US and northeast Canada were anomalously warm. The winter of 2013/14 was punctuated by several cold air outbreaks, the most severe of which occurred around the 7 January 2014. Compared to the daily average for this date in period 1980-99, the largest anomalies on 7 January 2014 were experienced in the eastern US, with -20°C anomalies stretching from Ohio as far south as Florida (Fig. 1b). Averaged over central to eastern North America (CENA; 70-100°W, 26-58°N; black box in Fig. 1b) daily mean temperatures were well below average for large portions of the winter (Fig. 1c). The coldest daily-mean temperature over CENA during the winter of 2013/14 occurred on 7 January, recording -16.8°C. On this day, temperatures averaged below -20°C over central Canada and west of the Great Lakes, and below -10°C over most of the US east of the Rockies (Fig. 1d).

Next, we consider how "extreme" the cold conditions were over CENA on 7 January 2014. Figure 2a shows the probability distribution function (PDF) of daily-mean temperatures, averaged over CENA, during the winter months of the late twentieth century (1980-99). The vertical green line is drawn at -16.8°C, corresponding to the mean temperature on 7 January 2014. The 7 January event falls in the tail of the distribution, but is not unprecedented in the recent past. The coldest day over this period occurred on 19 January 1994 (-20.3°C). During 1980-99, twenty days had a daily-mean CENA temperature as cold or colder than -16.8°C, spread across six winters (Table 1). Such events have often occurred in clusters, with multiple days this cold in several years. Based on the 1980-99 PDF (Fig. 2a), the 7 January 2014 event has a probability of 1.1%, which equates to an average return period of 1 year (since there are 90 winter days per year). Viewed in this light, the recent event does not seem to be a rare occurrence.

At first glance it may seem odd that so many long-term station records were broken on the 7 January 2014, if an event of such severity is not uncommon. However, the records referred to in the opening paragraph, and comparable records widely quoted in the media reporting of this event, refer to the fact that the temperature on the 7 January 2014 was colder than those on the same date in previous years, but not necessarily colder than on all dates in previous years. Cold extremes occur throughout the winter and not always on the same date. For example, days equally cold or colder than -16.8°C over CENA since 1980 have occurred on dates from mid December to early February (Table 1), but only once on the 7th of January – and that was in 2014. The probability of a cold extreme occurring on a particular date is therefore, much smaller than the probability of it occurring on any date. Hence, the breaking of records for a particular date is not necessarily a good measure of how "extreme" an event is.

A somewhat different perspective on the extremity of the 7 January event arises if a more recent reference period is considered. Figure 2b shows an analogous PDF based on daily winter CENA temperature during the period 2000-13. Arctic sea ice loss has accelerated in this period (Stroeve et al., 2012), so if there were a detectable influence of sea ice loss on cold extremes, we would expect to see it over this time period. Between 2000-2013, only one day (16 January 2009) was colder than -16.8°C, giving a probability of 0.08% (1 day in 14 years). Thus, the 7 January 2014 event could be perceived as "extreme" compared to temperature minima in the early twenty-first century, which may help explain the media and public perception of this event being "extreme". However, clearly this event was not uncommon in a longer-term context. Only a decade or two earlier, events of comparable magnitude occurred relatively frequently. This simple comparison suggests that cold extremes are becoming less frequent, not more frequent, consistent with previous studies (Alexander et al., 2006; Donat et al., 2013) and the anticipated response to global warming (Kharin et al., 2007; 2013). However, such interpretation must be treated with caution as the time periods considered are very short with few extremes (by definition) upon which to calculate robust statistics.

MODELS AND SIMULATIONS

We now turn our attention to quantifying future changes in CENA cold extremes, with particular focus on the projected changes driven by continued Arctic sea ice loss. To do this, we analyze large ensembles of coupled model simulations that have been forced by greenhouse gas (GHG) increases and which produce reductions in Arctic sea ice (Stroeve et al., 2012), amongst other impacts, and ensembles of atmospheric model simulations forced by solely the GHG-induced Arctic sea ice loss with all other forcing factors held constant.

To estimate the response to projected increases in GHG, we utilize coupled climate model simulations from fifth Coupled Model Intercomparison Project (CMIP5; Taylor et al., 2012). We chose to use the RCP8.5 concentration pathway, which is a high-end ("business-as-usual") scenario with a rapid rise in GHG concentrations through the twenty-first century, for two reasons: firstly, to maximize the signal-to-noise ratio and secondly, because observed Arctic sea ice reductions track those simulated under RCP8.5 more closely than those under any of the lower-end scenarios (Stroeve et al., 2012). We sample the projections at two time periods, 2030-49 and 2080-99, representative of the mid twenty-first century (C21) and late C21, respectively. The projections are compared to the baseline period 1980-99, representative of the late twentieth century (C20). Data for this period come from the CMIP5 historical simulations of the models. The historical simulations have all been forced with observed concentrations of GHG, aerosols, ozone and natural forcings (solar, volcanic eruptions) from 1850 to 2005. We analyzed one ensemble member from each of 34 models that had all necessary data available for the historical and RCP8.5 experiments.

To isolate the influence of sea ice, we performed atmospheric model simulations with prescribed sea ice concentration, sea ice thickness and sea surface temperature (SST). For this we used the atmospheric components of Hadley Centre Global Environmental Model version 2 (HadGEM2; Collins et al., 2011) and Community Climate System Model version 4 (CCSM4; Gent et al., 2011), namely the Hadley Centre Global Atmospheric Model version 2 (HadGAM2) and the Community Atmosphere Model version 4 (CAM4), respectively. The version of HadGAM2 used here has a horizontal resolution of 1.875° longitude by 1.25° latitude and 38 vertical levels. CAM4 has a horizontal resolution of 1.25° longitude by 0.9° latitude and 26 vertical levels. We performed three experiments using both models, each experiment having repeating seasonal cycles of sea ice conditions representative of a different time period - the late C20, mid C21 and late C21 (as defined above). These sea ice conditions were taken from the CMIP5 integrations of HadGEM2-ES and CCSM4 (i.e. sea ice from HadGEM2-ES was prescribed in HadGAM2 and sea ice from CCSM4 was prescribed in CAM4), averaged across the twenty years of the chosen period and all available ensemble members. Specifically, we used 5 HadGEM2-ES historical runs, 4 HadGEM2-ES RCP8.5 runs, 6 CCSM4 historical runs and 6 CCSM4 RCP8.5 runs. In the HadGAM2 experiments, sea ice thickness was derived empirically from the sea ice concentrations. In the CAM4 simulations, the prescribed sea ice thicknesses were based on climatologies from the CCSM4 simulations for each period (late C20, mid C21 and late C21; i.e., in the same manner as the sea ice concentrations). The treatment of SST was as follows. In the C20 experiment, sea surface temperatures (SST) were held to the climatology of the late C20, using the ensemble-mean SST from the HadGEM2-ES and CCSM4 historical simulations. In the mid and late C21 experiments, SST was also held to the climatology of the late C20, except at grid-boxes where sea ice was lost. At these locations, the climatological SST of the mid C21 or late C21 was used, taken from the HadGEM2-ES and CCSM4 RCP8.5 ensemble means. This procedure accounts for the local SST warming associated with reduced sea ice cover, but excludes remote SST changes that are not directly tied to the ice loss (see Screen et al., 2013; Deser et al., 2014). The three experiments were each run for 260 years. In this modeling framework, each model year can be considered an independent ensemble member starting from a different atmospheric initial condition. By running very large ensembles, we aim to fully capture the large intrinsic atmospheric variability. The details of each model experiments are summarized in Table 2.

CONTINUED ARCTIC SEA ICE LOSS

Ensemble-mean winter sea ice concentrations in HadGEM2-ES during the late C20, mid and late C21 are shown in Figure 3a-c, respectively. The projected loss of sea ice in the mid C21, relative to the late C20, is fairly small (-1.5 million km^2). The largest local changes in sea ice cover are found in the Barents Sea (cf. Fig. 3a,b). By late C21 however, HadGEM2-ES simulates almost ice-free conditions in winter (Fig. 3c). Ice cover is maintained predominantly in coastal regions and embayments. Analogous plots for CCSM4 are shown in Figure 3d-f. CCSM4 also simulates a modest change in winter sea ice cover between the late C20 and mid C21 (-1.3 million km^2). The largest changes in sea ice cover in CCSM4, in the late C21 relative to the late C20, are found in the Bering, Beaufort and Chukchi Seas

(Fig. 3f). In the late C21, CCSM4 simulates considerably more winter ice (8.6 million km^2) than HadGEM2-ES (3.5 million km^2). The change in winter sea ice area between the late C20 and late C21 is –10.3 and -4.8 million km^2, as simulated by HadGEM2-ES and CCSM4, respectively.

Figure 3g shows the winter sea ice area changes in these two models overlaid on the projected changes in all the CMIP5 models. In the late C20 and mid C21, both models have a winter sea ice cover close to the CMIP5 ensemble mean. In the late C21, the two models diverge from the CMIP5 mean. HadGEM2-ES simulates considerably less winter ice than the CMIP5 mean, whereas CCSM4 simulates more winter ice than the CMIP5 mean. Both models however, lie within the 10-90% range of the CMIP5 model spread. Thus, we consider the simulations by these two models to capture some of the uncertainty in future sea ice cover, but neither of the models are obvious outliers. In terms of winter sea ice volume, CCSM4 lies near to the CMIP5 mean in all three time periods (Fig. 3h). HadGEM2-ES has a winter sea ice volume close to the CMIP5 mean in the late C20 and late C21, but has a larger volume in the mid C21 (primarily due to thicker ice). We note that the sea ice thicknesses used to calculate these values are those derived empirically from the sea ice concentration (and prescribed to HadGAM2; see above) and not those simulated in the HadGEM2-ES RCP8.5 experiment.

WARMER AND LESS VARIABLE

Figure 4a shows PDFs of winter daily CENA temperature from 34 CMIP5 models. The three histograms show distributions based on the late C20 (grey bars), mid

C21 (blue) and late C21 (red). Each histogram is based upon 61,200 daily values (34 models x 20 years x 90 days). As a group, the CMIP5 models project a shift towards the right and a narrowing of the PDF, the former implying mean warming and the latter less variability. The mean warming measures 2.6°C by mid C21 and 6.5°C by late C21, both relative to the late C20. The standard deviation decreases by -0.3°C by mid C21 and by -0.7°C by late C21, again relative to the late C20. All these changes are statistically significant (95% confidence).

Figure 4b,c shows analogous PDFs from simulations of the HadGEM2-ES and CCSM4 models, respectively. We present the simulations from HadGEM2-ES and CCSM4 here to enable direct comparisons with the sea ice forced runs that were conducted with the atmospheric components of these coupled models. Both models show broadly the same response as the CMIP5 ensemble, namely mean warming and a decrease in variability. The HadGEM2-ES simulations show warming of 3.5°C and 8.7°C in the mid and late C21, respectively, and variability declines of -0.3°C and -1.1°C in the mid and late C21, respectively. The CCSM4 simulations show a mean warming of 2.6°C by mid C21 and 5.7°C by late C21, and a standard deviation decrease of -0.24°C by mid C21 and -0.58°C by late C21. Again, all quoted changes are statistically significant (95% confidence).

The results from the sea ice forced experiments are shown in Figure 4d,e, for HadGAM2 and CAM4 respectively. As under GHG forcing, the sea-ice forced simulations show mean warming and a decrease in variability, but to a lesser degree than in the GHG forced experiments. The sea ice forced changes in mean temperature and standard deviation are relatively small between the late C20 and mid C21, but emerge more clearly by the late C21, consistent with the magnitude of the sea ice loss (recall Fig. 3g). HadGAM2 simulates warming of 0.3°C by mid C21 and 2.0°C by late C21, and CAM4 exhibits warming of 0.7°C and 2.2°C, respectively (all statistically significant). These CENA temperature changes can be divided by the changes in winter sea ice area to yield sensitivity terms. In HadGAM2 this sensitivity is 0.2°C/million km^2 (multiplied by -1 to yield a value for sea ice area loss) between the late C20 and mid C21, and the ssame value between the mid and late C21. In CAM4 the corresponding values are 0.5 and 0.4°C/million km^2. Thus, in both models there is an approximately linear relationship between winter sea ice area loss and CENA warming; however, CAM4 has a higher sensitivity than HadGAM2. Both models simulate a statistically significant decrease in the standard deviation of CENA temperature by late C21 in response to sea ice loss, -1.0°C in HadGAM2 and -0.8°C in CAM4, which represents a 27% and 18% decrease relative to the late C20, respectively. Although much smaller in magnitude, a statistically significant decrease in variability in response to sea ice loss is evident by mid C21 in both models. None of the C21 sea ice forced experiments show evidence of cooling or increased variability relative to the C20: in other words, there is no evidence for increased cold extremes.

So, why does Arctic sea ice loss make CENA temperature warmer and less variable? Arctic sea ice loss drives local warming via changes in the surface heat fluxes (Deser et al., 2010; Screen and Simmonds, 2010a,b; Screen et al., 2013). This warming signal is spread to lower latitudes primarily due to temperature advection by transient eddies (Deser et al., 2010). Temperature advection can also help explain the variability decrease. Cold winter days in mid-latitudes tend to coincide with northerly wind (from the Arctic) and warm winter days with southerly wind (from the sub-tropics). Arctic warming, induced by sea ice loss, leads to warmer northerly wind but little change in temperature of southerly wind (Screen, 2014). As a result, cold days warm faster than warm days, leading to a decrease in daily temperature variability (Screen, 2014). Figure 4 clearly shows that the cold (left-hand) tail of the CENA temperature PDF warms more (i.e., shifts further to the right) than does the warm (right-hand) tail, supporting this simple mechanism.

Contrasting the GHG forced and sea ice forced simulations, sea ice loss in HadGAM2 explains 9% of the mean warming and 52% of the decreased standard deviation seen in HadGEM2-ES between the late C20 and mid C21, and sea ice loss in CAM4 account for 25% of the mean warming and 58% of the decreased standard deviation seen in CCSM4 in the CENA region (Table 3). By late C21, sea ice loss accounts for 24% of the mean warming and 87% of the decreased standard deviation in HadGEM2-ES, and 38% of the mean warming and 141% of the decreased standard deviation in CCSM4. The latter percentage, being larger than 100%, implies that other processes (not directly related to Arctic sea ice loss) in the GHG forced experiment are responsible for an increase in variability that partially offsets the sea ice driven variability decrease. Evidently Arctic sea ice loss is the key driver of the projected decrease in variability by late C21, supporting similar conclusions for the mid-latitudes as a whole (Screen, 2014).

REDUCED RISK OF COLD EXTREMES

For each experiment, we identified a threshold CENA temperature that occurs with 1.1% (1 day per year) frequency during the late C20. This represents the model analogue to the 7 January 2014. We note that because the models are generally biased cold relative to the reanalysis, the chosen threshold temperatures are lower than -16.8°C (-18.7°C, -20.5°C, -18.6°C, –17.1°C, and -18.5°C for the CMIP5, HadGEM2-ES, CCSM4, HadGAM2 and CAM4 simulations, respectively). Figure 4f shows how the probability of CENA temperature equal to or below this threshold changes in the future in response to increased GHG and to Arctic sea ice loss. In the CMIP5 models, the probability reduces to 0.21% (1 day in 5 years) by the mid C21. By the late C21, CENA temperature never equals or falls below the threshold. In the HadGEM2-ES coupled simulations, the probability reduces to 0.014% (1 day in 80 years) by the mid C21 and again, reduces to zero by the late C21. The probability reduces to 0.093% (1 day in 12 years) and zero in the CCSM4 simulations, by mid C21 and late C21 respectively. Thus by mid C21, increased GHG reduce the odds of an event as severe as 7 January 2014 by a factor of 5 based on the CMIP5 models as a group, a factor of 80 based on HadGEM2-ES, and a factor of 12 based on CCSM4.

In response to projected sea ice loss, the probability of CENA temperature below the threshold temperature reduces to 0.7% (1 day in 1.6 years) in HadGAM2 and to 0.8% (1 day in 1.4 years) in CAM4 by mid C21. Thus, projected Arctic sea ice loss alone reduces the odds of such an event by one quarter to one third in the mid C21 compared to late C20. By late C21, the probability falls to zero in HadGAM2 and 0.06% (1 day in 19 years) in CAM4.

The sea-ice forced simulations presented here were not coupled to an ocean model and thus, ocean feedbacks are not represented. Deser et al. (2014) examined the climate response to projected Arctic sea ice in coupled and uncoupled versions of CCSM4. These authors show that the coupled response to Arctic sea ice loss resembles a weaker version of the full response to GHG in CCSM4. Since North American warming and decreased temperature variance are robust characteristics of the full coupled response to GHG, we speculate that ocean feedbacks may further reduce the risk of cold extremes, or at least are unlikely to increase the risk.

HEMISPHERIC PERSPECTIVE

A wider geographical perspective on the simulated response to sea ice loss is provided in Figure 5, which shows maps of mean temperature and standard deviation change between the late C20 and mid C21. Both models show warming over the high-latitude continents (Fig. 5a,c), accompanied by a decrease in standard deviation (Fig. 5b,d). Both the warming and variability decrease are more widespread in CAM4 than in HadGAM2. By the late C21, both models depict larger warming over the high-latitude continents and an extension of the warming signal into parts of the mid-latitudes (Fig. 6). In particular, warming is simulated over much of eastern US. Also by late C21, there are larger magnitude and more widespread simulated reductions in standard deviation, with significant decreases over most of North America, Russia and northern Europe by late C21. In contrast, both models depict weak cooling and patches of increased standard deviation over eastern Asia (China, Mongolia). This cooling is related to a simulated strengthening of the Siberian High (not shown), consistent with the model results of Mori et al (2014). It is noteworthy that the two models depict a robust spatial pattern of mean temperature and variability change in response to Arctic sea ice loss.

These changes in mean temperature and variability due to Arctic sea ice loss would be expected to translate into altered frequencies of cold extremes. To show this explicitly, Figure 7 presents the spatial pattern of the sea ice forced change in the probability of cold extremes. Here the temperature threshold is calculated as the 1.1-percentile of the late C20 distribution at each grid point. For clarity in Figure 7, we simplify these probability changes into broad categories that emphasize the sign and relative magnitude of the sea ice forced change from the late C20. Focusing first on the changes by mid C21, both models depict reduced probabilities of cold extremes over the high-latitudes (Fig. 7a,c). The mid-latitude responses are dissimilar in the two models. For example, HadGAM2 shows reduced probability over the majority of North America whereas CAM4 depicts comparably large reductions over northern and eastern North America, but modest increases over southern and western parts of the continent. The late C21 changes are in very good agreement between the models, however (Fig. 7b,d). This suggests that the discrepancies in the mid C21 responses arise due to the small signal-to-noise ratio and not model differences in the forced response. By late C21 both models simulate large probability reductions over North

America, Europe and Russia. In parts of northern Canada and northeast Asia the probability reduces to zero and over large swaths of North America and northern Asia the probability is more than halved. Both models show slightly increased probabilities over central and southern Asia, although the exact regions differ, related cooling induced by a strengthened Siberian High.

So far we have only considered the changing probability of extremely cold days. There has been recent speculation that Arctic warming and sea ice loss may increase the frequency of longer-duration cold extremes as a result of more persistent weather patterns over North America (Francis and Vavrus, 2012). Motivated by this, we have also examined the changing probability of 5-day and 9-day cold extremes (Figure 8). The simulated changes in the frequency of these longer-duration extremes closely match those shown previously for daily extremes (as do the patterns of standard deviation change; not shown). Therefore, our simulations do not support the hypothesis of more frequent cold spells over central and eastern North America in response to sea ice loss. They do suggest that, in isolation, Arctic sea ice loss favors increased cold spells over central Asia, consistent with Mori et al (2014). However, it should be noted that the net effect of GHG increases is to reduce the chance of central Asian cold extremes (Mori et al., 2014).

CONCLUDING REMARKS

We have used large ensembles of model simulations to explore how the risk of North American daily cold extremes is anticipated to change in the future, in response to increases in GHG and the component of that response due solely to Arctic sea ice loss. Specifically, we have examined the changing probability of daily cold extremes as (un)common as the 7 January 2014 event. Projected increases in GHG will decrease the likelihood of North American cold extremes in the future. Days as cold or colder than the 7 January 2014 are still projected to occur in the mid C21 (2030-49), albeit less frequently than in the late C20 (1980-99). However, such events will cease to occur by the late C21 (2080-99), assuming GHG emissions continue unabated. Continued Arctic sea ice loss is a major driver of decreased - not increased - North America cold extremes. Projected Arctic sea ice loss alone reduces the odds of such an event by one quarter to one third in the mid C21 compared to late C20, and to zero (or near-zero) by the late C21. Both projected mean warming and a decrease in temperature variability contribute to the decrease in daily cold extremes.

Recent claims that Arctic sea ice loss may increase the risk of mid-latitude cold extremes are primarily based on hypothesized increases in the latitudinal extent of north-south excursions of the Jetstream. The simple reasoning is that a more meandering Jetstream will increase the frequency of cold Arctic air migrating southwards and thus, lead to more frequent cold extremes in the mid-latitudes. However, this logic ignores two important factors, even putting aside the considerable uncertainty in future changes in the Jetstream (Barnes and Polvani, 2013) and associated features of the atmospheric circulation (Masato et al., 2013). The first factor ignored is that the mid-latitudes are warming. This means it takes a larger magnitude cold anomaly to cause a cold extreme than in a cooler climate. The second factor ignored is that disproportionally large warming of the high-latitudes compared to the mid-latitudes reduces the average temperature gradient between these two regions. This means that if an Arctic air mass is displaced southward into the mid-latitudes, the resulting temperature anomaly is smaller than is the case for a larger north-south temperature gradient. These two factors translate into a reduced chance of cold extremes. Our results suggest these thermodynamically induced changes are of first-order importance in determining the future risk of cold extremes, and that dynamically induced changes play a secondary role (such as changes in the behavior of the Jetstream). As a result, we should expect fewer - and not more - cold extremes over the coming decades in the mid-latitudes including North America.

ACKNOWLEDGEMENTS

Michael Alexander and three anonymous reviewers are thanked for their time and feedback. We thank Robert A. Tomas for conducting some of the CAM4 simulations. The HadGAM2 simulations were performed on the ARCHER UK National Supercomputing Service. James Screen is supported by UK National Environmental Research Council grant NE/J019585/1. Lantao Sun is supported by a grant from the U.S. National Science Foundation Office of Polar Programs. NCAR is sponsored by the U.S. National Science Foundation.

REFERENCES

Alexander L V et al 2006 Global observed changes in daily climate extremes of temperature and precipitation *J. Geophys. Res.* **111** D05109

Barnes E A 2013 Revisiting the evidence linking Arctic amplification to extreme weather in midlatitudes *Geophys. Res. Lett.* **40** 4728-4733

Barnes E A, Dunn-Sigouin E, Masato G and Wooling T 2014 Exploring recent trends in Northern Hemisphere blocking *Geophys. Res. Lett.* **41** 638-644

Barnes E A and Polvani L M 2013 Response of the midlatitude jets and of their variability to increased greenhouse gases in the CMIP5 models *J. Clim.* **26** 7117-7135

Cohen J, Screen J A, Furtado J C, Barlow M, Whittlestone D, Coumou D, Francis J, Dethloff K, Entekhabi D, Overland J and Jones J 2014 The relationship between recent Arctic amplification and extreme mid-latitude weather *Nature Geosc.* accepted

Collins W J and Coauthors 2011 Development and evaluation of an Earth-System model – HadGEM2 *Geophys. Model Dev.* **4** 1051-1075

Deser C, Tomas R, Alexander M and Lawrence D 2010 The seasonal atmospheric response to projected Arctic sea ice liss in the late 21st century *J. Clim.* **23** 333-351

Deser C, Tomas R and Sun L 2014 The role of ocean-atmosphere coupling in the zonal-mean atmospheric response to Arctic sea ice loss *J. Clim.* submitted

Donat M G et al 2013 Updated analyses of temperature and precipitation extreme indices since the beginning of the twentieth century: the HadEX2 dataset *J. Geophys. Res.* **118** 2098-2118

Fischer E M and Knutti R 2014 Heated debate on cold weather *Nature Clim. Change* **4** 537-538

Francis J A and Vavrus S J 2012 Evidence linking Arctic amplification to extreme weather in mid-latitudes *Geophys. Res. Lett.* **39** L06801

Gent P R and Coauthors 2011 The Community Climate System Model Version 4 *J. Clim.* **24** 4973-4991

Gerber F, Sedlacek J and Knutti R 2014 Influence of thes western North Atlantic and the Barents Sea on European winter climate *Geophys. Res. Lett.* **41** 561-567

Hassanzadeh P, Kuang Z and Farrell B F 2014 Responses of mid-latitude blocks and wave amplitude to change in the meridional temperature gradient in an idealized dry GCM *Geophys. Res. Lett.* accepted

Honda M, Inoue J and Yamane S 2009 Influence of low Arctic sea-ice minima on anomalously cold Eurasian winters *Geophys. Res. Lett.* **36** L08707

Hurrell J W 1995 Decadal trends in the North Atlantic Oscillations: Regional temperatures and precipitation *Science* **269** 676-679

Inoue J, Hori M E and Takaya K 2012 The role of Barents sea ice in the wintertime cyclone track and emergence of a warm-Arctic cold-Siberian anomaly *J. Clim.* **25** 2561–2568

Kalnay E and Coauthors 1996 The NCEP/NCAR 40-year reanalysis project *Bull. Amer. Meteor. Soc.* **77** 437-471

Kharin V V, Zwiers F W, Zhang X and Hegerl G C 2007 Change in daily temperature and precipitation extremes in the IPCC ensemble of global coupled model simulations *J. Clim.* **20** 1419-1444

Kharin V V, Zwiers F W, Zhang X and Wehner M 2014 Changes in temperature and precipitation extremes in the CMIP5 ensemble *Clim. Change* **81** 249-265

Liu J, Curry J A, Wang H, Song M and Horton R M 2012 Impact of declining Arctic sea ice on winter snowfall *Proc. Natl. Acad. Sci. USA* **109** 4074-4079

Masato G, Hoskins B and Woolings T 2013 Winter and summer Northern Hemisphere blocking in CMIP5 models *J. Clim.* **26** 7044-7059

Mori, M., M. Watanabe, H. Shiogama, J, Inoue and M. Kimoto 2014 Robust Arctic sea-ice influence on the frequent Eurasian cold winters in past decades *Nature Geosci.* Doi:10.1038/ngeo2277

Peings Y and Magnusdottir G 2014 Response of the wintertime Northern Hemisphere atmospheric circulation to current and projected Arctic sea ice decline: A numerical study with CAM5 *J. Clim.* **27** 244-264

Petoukhov V and Semenov V 2010 A link between reduced Barents-Kara sea ice and cold winter extremes over northern continents *J. Geophys. Res.* **115** D21111

Screen J A 2014 Arctic amplification decreases temperature variance in northern mid- to high-latitudes *Nature Clim. Change* **4** 577-582

Screen J A and Simmonds I 2010a The central role of diminishing sea ice in recent Arctic temperature amplification *Nature* **464** 1334-1337

Screen J A and Simmonds I 2010b Increasing fall-winter energy loss from the Arctic Ocean and its role in Arctic temperature amplification *Geophys. Res. Lett.* **37** L16797

Screen J A and Simmonds I 2013 Exploring links between Arctic amplification and mid-latitude weather *Geophys. Res. Lett.* **40** doi:10.1002/grl.50174

Screen J A, Simmonds I, Deser C and Tomas R 2013 The atmospheric response to three decades of observed Arctic sea ice loss *J. Clim.* **26** 1230-1248

Screen J A, Deser C, Simmonds I and Tomas R 2014 Atmospheric impacts of Arctic sea-ice loss, 1979–2009: separating forced change from atmospheric internal variability *Clim. Dyn.*

Stroeve J C Kattsov V, Barrett A, Serreze M, Pavlova T, Holland M and Meier W N 2012 Trends in Arctic sea ice extent from CMIP5, CMIP3 and observations *Geophys. Res. Lett.* **39** L16502

Tang Q, Zhang X, Yang X and Francis J A 2013 Cold winter extremes in northern continents linked to Arctic sea ice loss *Environ. Res. Lett.* **8** 014036

Taylor K E, Stouffer R J and Meehl G A A N 2012 Overview of CMIP5 and the experiment design *Bull. Amer. Meteor. Soc.* **93** 485-498

Vihma T 2014 Effects of Arctic sea ice decline on weather and climate: A review *Surv. Geophys.* Doi:10.1007/s10712-014-9284-0

Wallace J M, Held I M, Thompson D W, Trenberth K E and Walsh J 2014 Global warming and winter weather *Science* **343** 729-730

Walsh J 2014 Intensified warming if the Arctic: Causes and impacts on middle latitudes *Global and Planetary Change* **117** 52-63

Woolings T, Harvey B and Masato G 2014 Arctic warming, atmospheric blocking and cold European winter in CMIP5 models *Environ. Res. Lett.* **9** 014002

Yang S and Christensen J H 2012 Arctic sea ice reduction and European cold winters in CMIP5 climate change experiments *Geophys. Res. Lett.* **39** L20707

TABLES

Table 1: Days equally as cold or colder than 7 January 2014 over CENA since 1980, based on the NCEP-NCAR reanalysis.

Date	CENA T (°C)	Date	CENA T (°C)	Date	CENA T (°C)
25/12/80	-16.8	25/12/83	-20.2	18/1/94	-17.5
10/1/82	-18.2	20/1/84	-17.9	19/1/94	-20.3
11/1/82	-18.6	21/1/84	-17.4	1/2/96	-18.4
17/1/82	-20.1	22/12/89	-20.2	2/2/96	-18.2
19/12/83	-17.5	23/12/89	-19.6	3/2/96	-20.2
20/12/83	-17.2	15/1/94	-18.2	4/2/96	-19.8
24/12/83	-18.1	16/1/94	-18.4	16/1/09	-17.2

Table 2: Details of the model simulations analyzed.

Model(s)	**Forcing**	**Time period analyzed**	**Ensemble members**	**Years of simulation**
CMIP5	Historical	1980-1999	34^	680
	RCP8.5	2030-2049	34^	680
	RCP8.5	2080-2099	34^	680
HadGEM2-ES	Historical (**A**)	1980-1999	5	100
	RCP8.5 (**B**)	2030-2049	4	80
	RCP8.5 (**C**)	2080-2099	4	80
CCSM4	Historical (**D**)	1980-1999	3	60
	RCP8.5 (**E**)	2030-2049	6	120
	RCP8.5 (**F**)	2080-2099	6	120
HadGAM2	Mean sea ice from **A**, SST from **A**	Annually repeating	260	260
	Mean sea ice from **B**, SST from **A**	Annually repeating	260	260
	Mean sea ice from **C**, SST from **A**	Annually repeating	260	260
CAM4	Mean sea ice from **D**, SST from **D**	Annually repeating	260	260
	Mean sea ice from **E**, SST from **D**	Annually repeating	260	260
	Mean sea ice from **F**, SST from **D**	Annually repeating	260	260

^One ensemble member per model. The 34 CMIP5 models analyzed are: ACCESS1.0, ACCESS1.3, bcc-csm1.1, bcc-csm1.1m, BNU-ESM, CanESM2, CCSM4, CESM1-BGC, CESM1-CAM5, CMCC-CESM, CMCC-CM, CMCC-CMS, CNRM-CM5, CSIRO-Mk3.6.0, EC-EARTH, GFDL-CM3, GFDL-ESM2G, GFDL-ESM2M, GISS-E2-H, GISS-E2-R, HadGEM2-CC, HadGEM2-ES, inmcm4, IPSL-CM5A-LR, IPSL-CM5A-MR, IPSL-CM5B-LR, MIROC-ESM, MIROC-ESM-CHEM, MIROC5, MPI-ESM-LR, MPI-ESM-MR, MRI-CGCM3, MRI-ESM1 and NorESM1-M.

Table 3: Changes in winter daily mean CENA temperature and variance simulated in response to GHG increases and Arctic sea ice decreases. The numbers in parentheses denote the percentage of simulated change under GHG forcing that can be explained solely by projected Arctic sea ice loss. All changes are statistically significant at the 95% confidence level.

		Temperature change relative to 1980-1999 (°C)		**Standard deviation change relative to 1980-99 (°C)**	
Model	**Period**	**GHG**	**Sea ice**	**GHG**	**Sea ice**
HadGEM2-ES/ HadGAM2	2030-49	3.49	0.32 (9%)	-0.31	-0.16 (52%)
	2080-99	8.67	2.08 (24%)	-1.11	-0.97 (87%)
CCSM4/CAM4	2030-49	2.62	0.65 (25%)	-0.24	-0.14 (58%)
	2080-99	5.74	2.17 (38%)	-0.58	-0.82 (141%)

FIGURE CAPTIONS

Figure 1. North American temperature anomalies for (**a**) the winter of 2013/14 and (**b**) 7 January 2014. Anomalies are relative to the period 1980-99. (**c**) Daily-mean temperature averaged over CENA (black box in **b**) for 1 November 2013 to 31 March 2014 (black curve) and the daily 1980-99 climatology (grey). Blue (orange) shading shows days colder (warmer) than the average for that day. (**d**) North American temperatures for 7 January 2014.

Figure 2. (**a**) Histogram of daily winter temperatures averaged over CENA during the period 1980-99. (**b**) As **a**, but based on the period 2000-13. The green lines are drawn at -16.8°C and correspond to the temperature on 7 January 2014. The numbers in the top left and right of each panel are the mean temperature and standard deviation, respectively, in units of °C.

Figure 3. Ensemble-mean winter sea ice concentrations from HadGEM2-ES during the period (**a**) 1980-99, (**b**) 2030-49 and (**c**) 2080-99. (**d-f**) As **a-c**, but for CCSM4. (**g**) Evolution of winter sea ice area in the CMIP5 historical and RCP8.5 experiments, 1980-2099. The blue curve denotes the multi-model mean, dense hatching the 10-90% range of the model spread and light hatching the full model spread. The black and green lines show the values prescribed in the sea ice forced HadGAM2 and CAM4 simulations, respectively. (**h**) As **g**, but for sea ice volume.

Figure 4. (**a**) Histograms of simulated daily winter temperature averaged over CENA taken from 34 coupled climate models for the periods 1980-99 (grey bars), 2030-49 (blue) and 2088-99 (red). The numbers in the top left and right of each panel are the mean temperature and standard deviation, respectively, in units of °C. The vertical green line denotes the value of the model's 1.1 percentile, the simulated analog of the 7 January 2014 event in observations. (**b-e**) As **a**, but for coupled simulations with (**b**) HadGEM2-ES and (**c**) CCSM4, and for sea ice forced simulations with (**d**) HadGAM2 and (**e**) CAM4. (**f**) The probability of daily temperature as cold or colder than the 1.1 percentile in the period 1980-1999 in each model ensemble and time period.

Figure 5. Differences in (**a**) mean winter near-surface air temperature and (**b**) standard deviation of daily winter near-surface air temperature, between the period 2030-49 and 1980-99 in the HadGAM2 sea ice forced experiments. (**c-d**) As **a-b**, but for the CAM4 sea ice forced experiments. Colored shading is shown only at grid-points where the difference is statistically significant at the 95% confidence level.

Figure 6. As Figure 5, but for differences between the period 2080-99 and 1980-99. Note the different color scales.

Figure 7. (**a**) Probability of extreme cold (defined as a winter daily temperature as cold or colder than the 1.1-percentile during the period 1980-99) in the sea ice forced HadGAM2 simulation for the period 2030-49. The colored shading categories are based on the relative change in probability compared to the

period 1980-99. (**b**) As **a**, but for the period 2080-99 relative to 1980-99. (**c-d**) As **a-b**, but for the sea ice forced CAM4 simulations.

Figure 8. (**a**) Probability of extreme cold (defined as a winter 5-day mean temperature as cold or colder than the 1.1-percentile during the period 1980-99) in the sea ice forced HadGAM2 simulation for the period 2080-99. The colored shading categories are based on the relative change in probability compared to the period 1980-99. (**b**) As **a**, but for 9-day means. (**c-d**) As **a-b**, but for the sea ice forced CAM4 simulations.

FIGURES

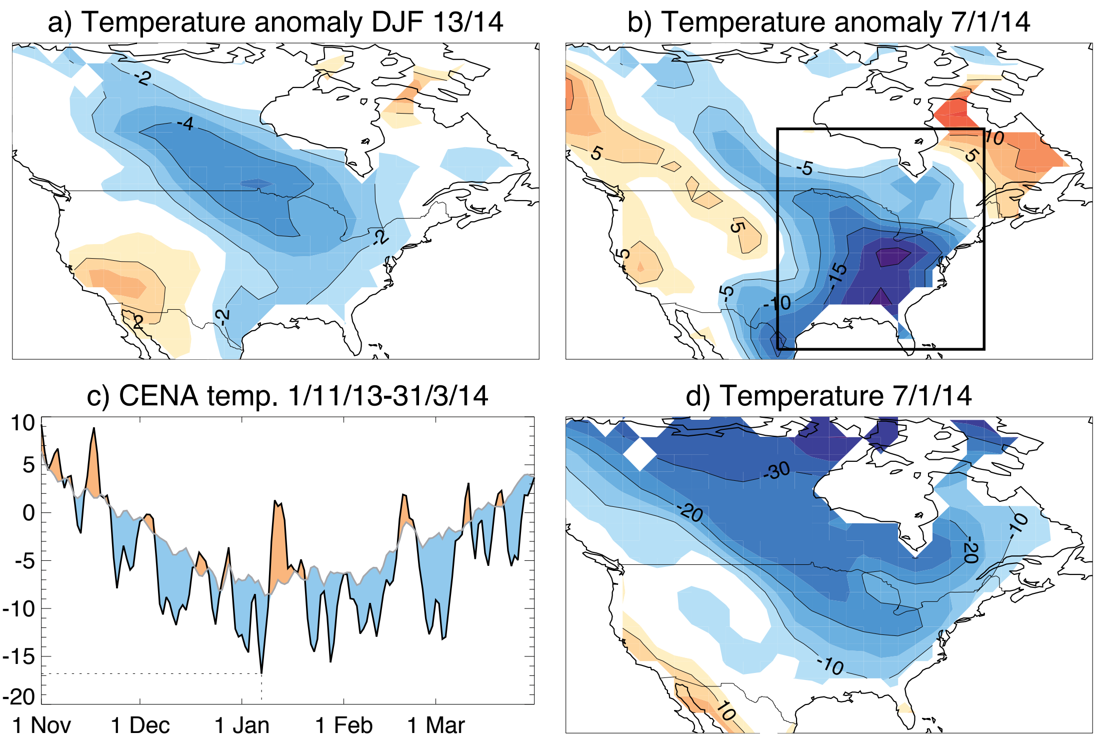

Figure 1. North American temperature anomalies for (**a**) the winter of 2013/14 and (**b**) 7 January 2014. Anomalies are relative to the period 1980-99. (**c**) Daily-mean temperature averaged over CENA (black box in **b**) for 1 November 2013 to 31 March 2014 (black curve) and the daily 1980-99 climatology (grey). Blue (orange) shading shows days colder (warmer) than the average for that day. (**d**) North American temperatures for 7 January 2014.

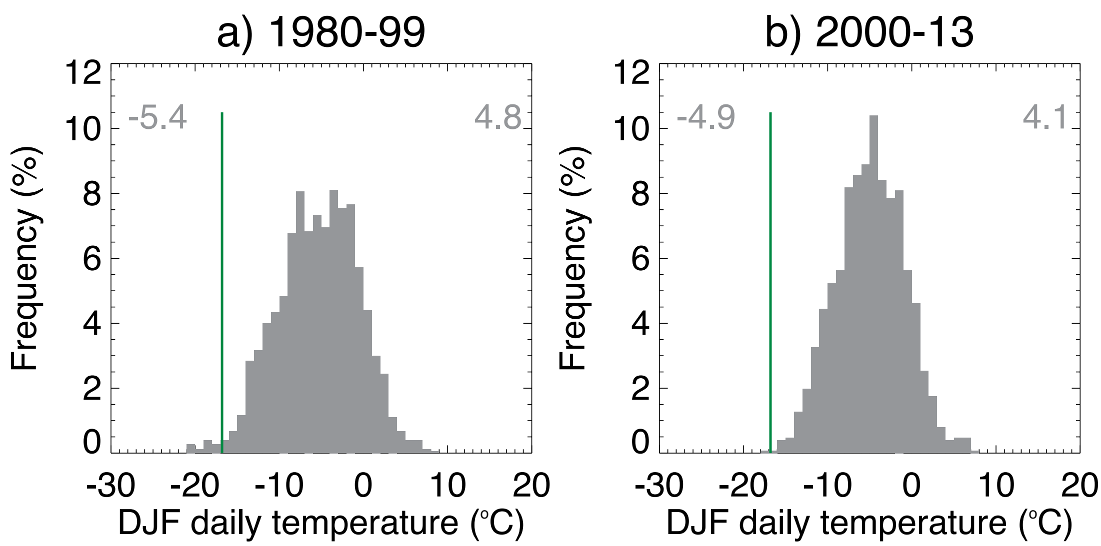

Figure 2. (**a**) Histogram of daily winter temperatures averaged over CENA during the period 1980-99. (**b**) As **a**, but based on the period 2000-13. The green lines are drawn at -16.8°C and correspond to the temperature on 7 January 2014. The numbers in the top left and right of each panel are the mean temperature and standard deviation, respectively, in units of °C.

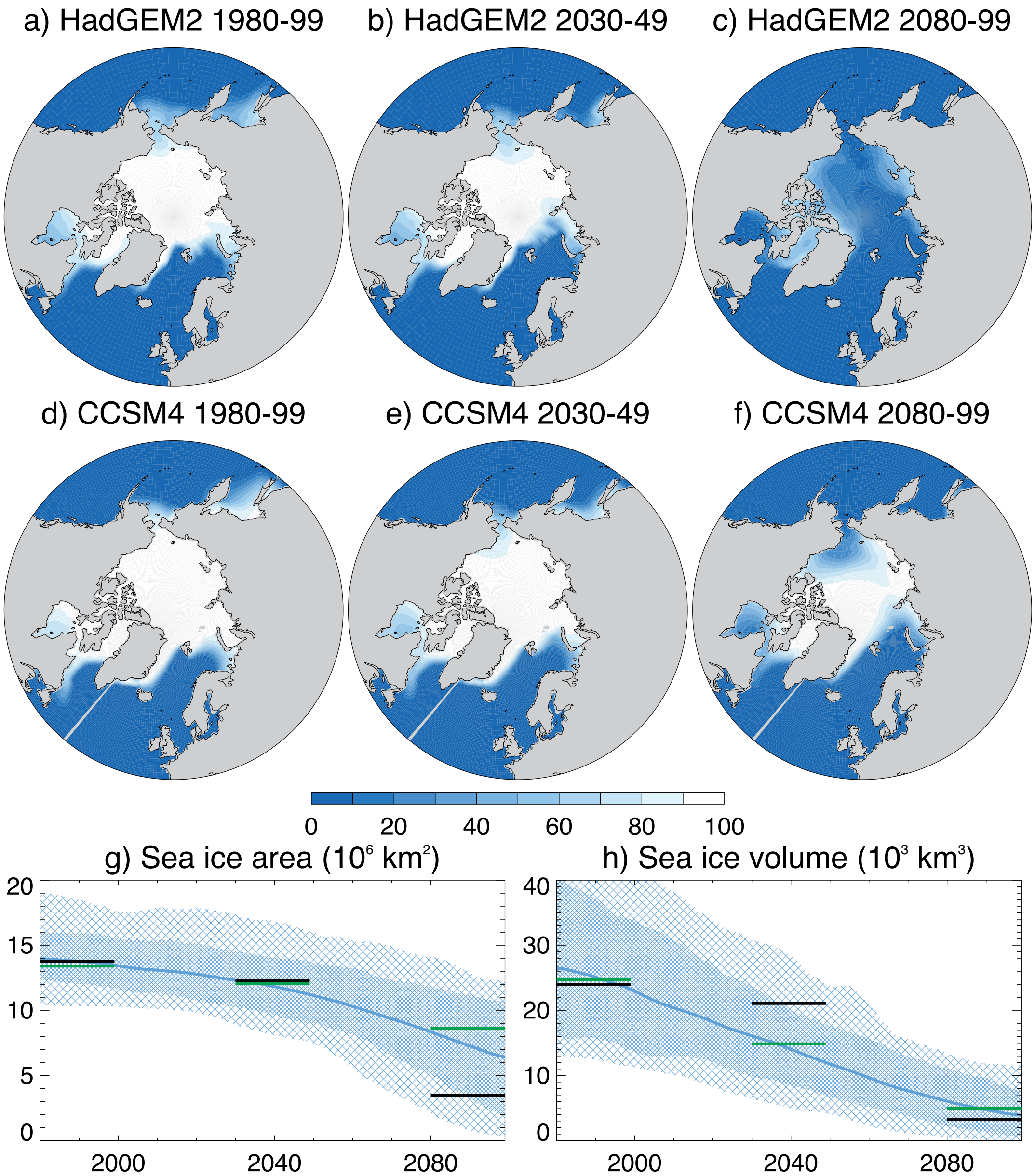

Figure 3. Ensemble-mean winter sea ice concentrations from HadGEM2-ES during the period (**a**) 1980-99, (**b**) 2030-49 and (**c**) 2080-99. (**d-f**) As **a-c**, but for CCSM4. (**g**) Evolution of winter sea ice area in the CMIP5 historical and RCP8.5 experiments, 1980-2099. The blue curve denotes the multi-model mean, dense hatching the 10-90% range of the model spread and light hatching the full model spread. The black and green lines show the values prescribed in the sea ice forced HadGAM2 and CAM4 simulations, respectively. (**h**) As **g**, but for sea ice volume.

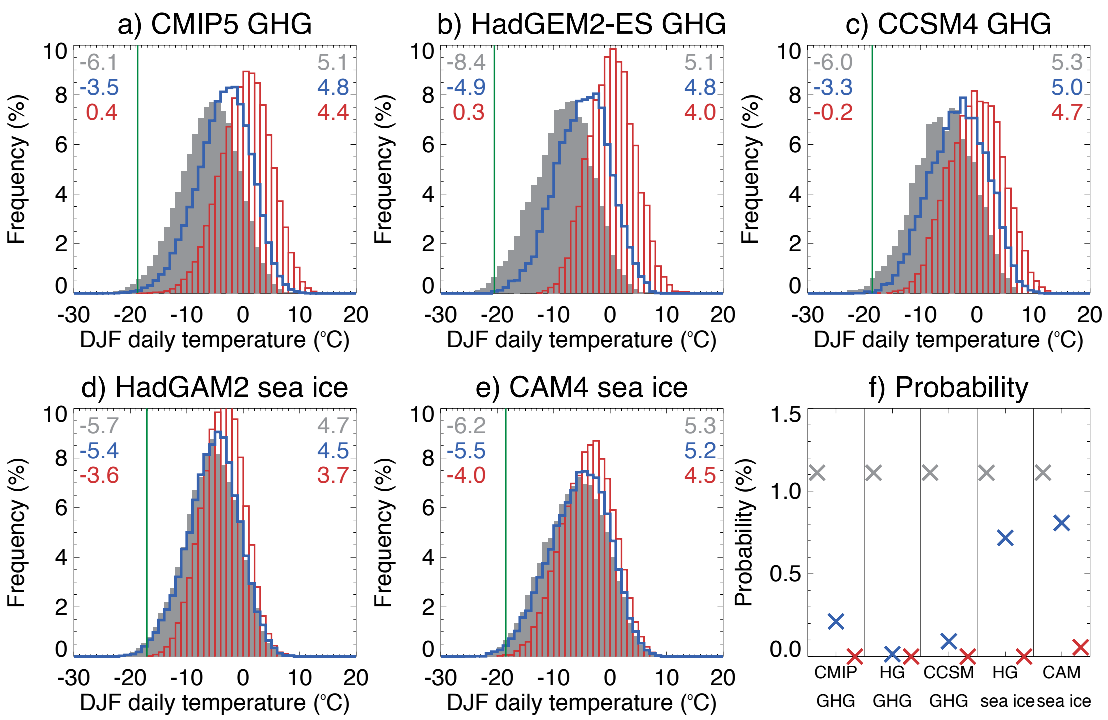

Figure 4. (**a**) Histograms of simulated daily winter temperature averaged over CENA taken from 34 coupled climate models for the periods 1980-99 (grey bars), 2030-49 (blue) and 2088-99 (red). The numbers in the top left and right of each panel are the mean temperature and standard deviation, respectively, in units of °C. The vertical green line denotes the value of the model's 1.1 percentile, the simulated analog of the 7 January 2014 event in observations. (**b-e**) As **a**, but for coupled simulations with (**b**) HadGEM2-ES and (**c**) CCSM4, and for sea ice forced simulations with (**d**) HadGAM2 and (**e**) CAM4. (**f**) The probability of daily temperature as cold or colder than the 1.1 percentile in the period 1980-1999 in each model ensemble and time period.

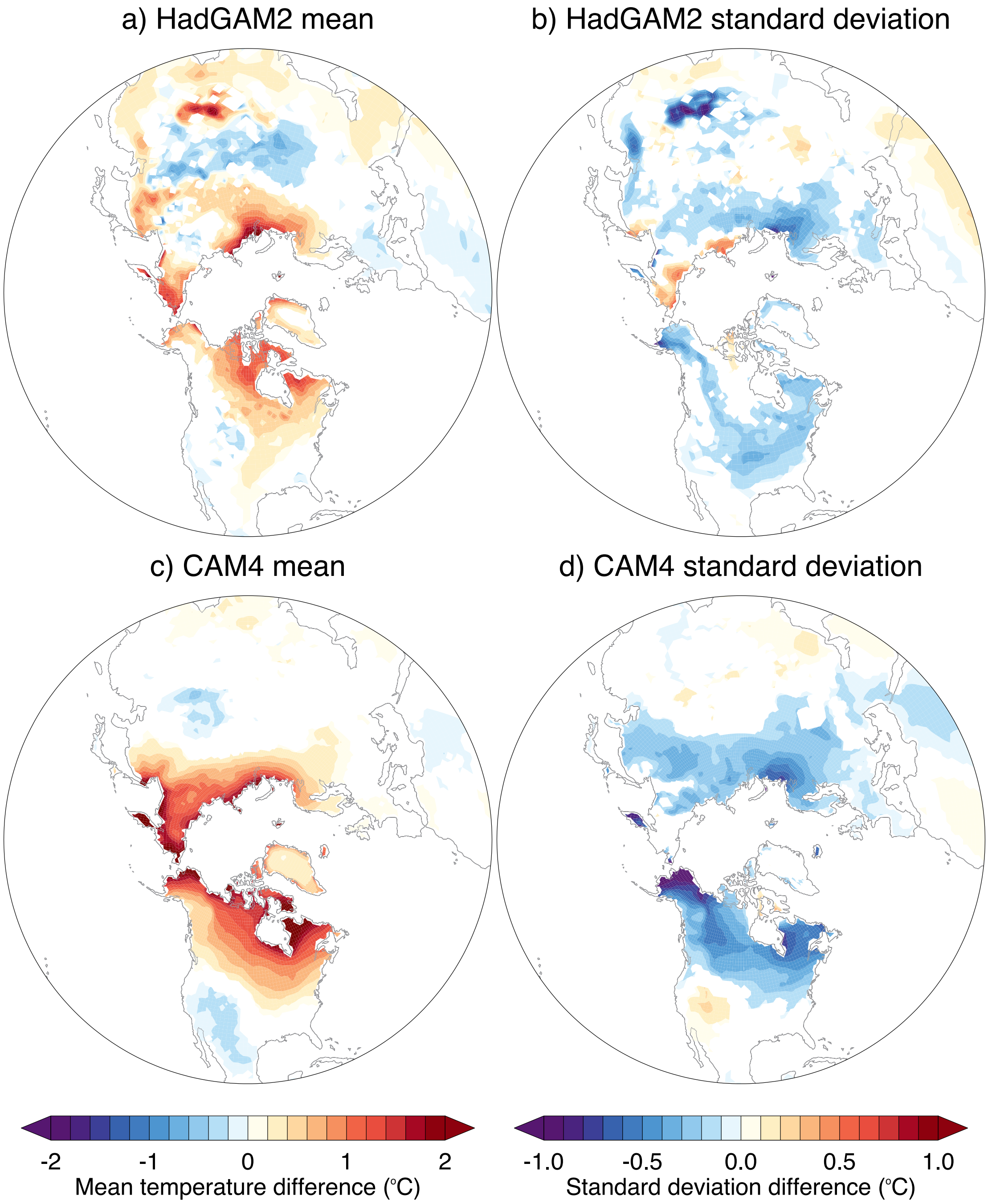

Figure 5. Differences in (**a**) mean winter near-surface air temperature and (**b**) standard deviation of daily winter near-surface air temperature, between the period 2030-49 and 1980-99 in the HadGAM2 sea ice forced experiments. (**c-d**) As **a-b**, but for the CAM4 sea ice forced experiments. Colored shading is shown only at grid-points where the difference is statistically significant at the 95% confidence level.

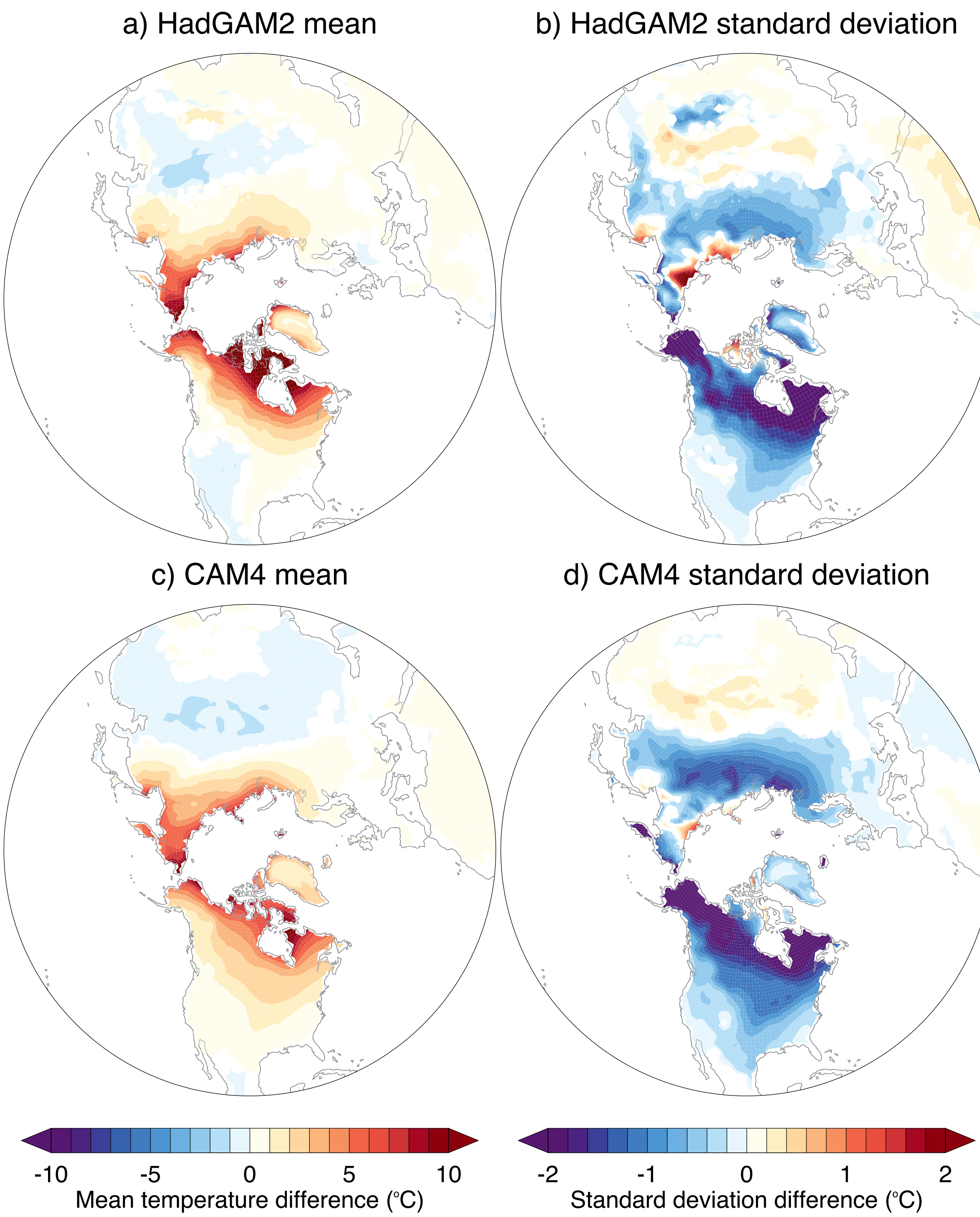

Figure 6. As Figure 5, but for differences between the period 2080-99 and 1980-99. Note the different color scales.

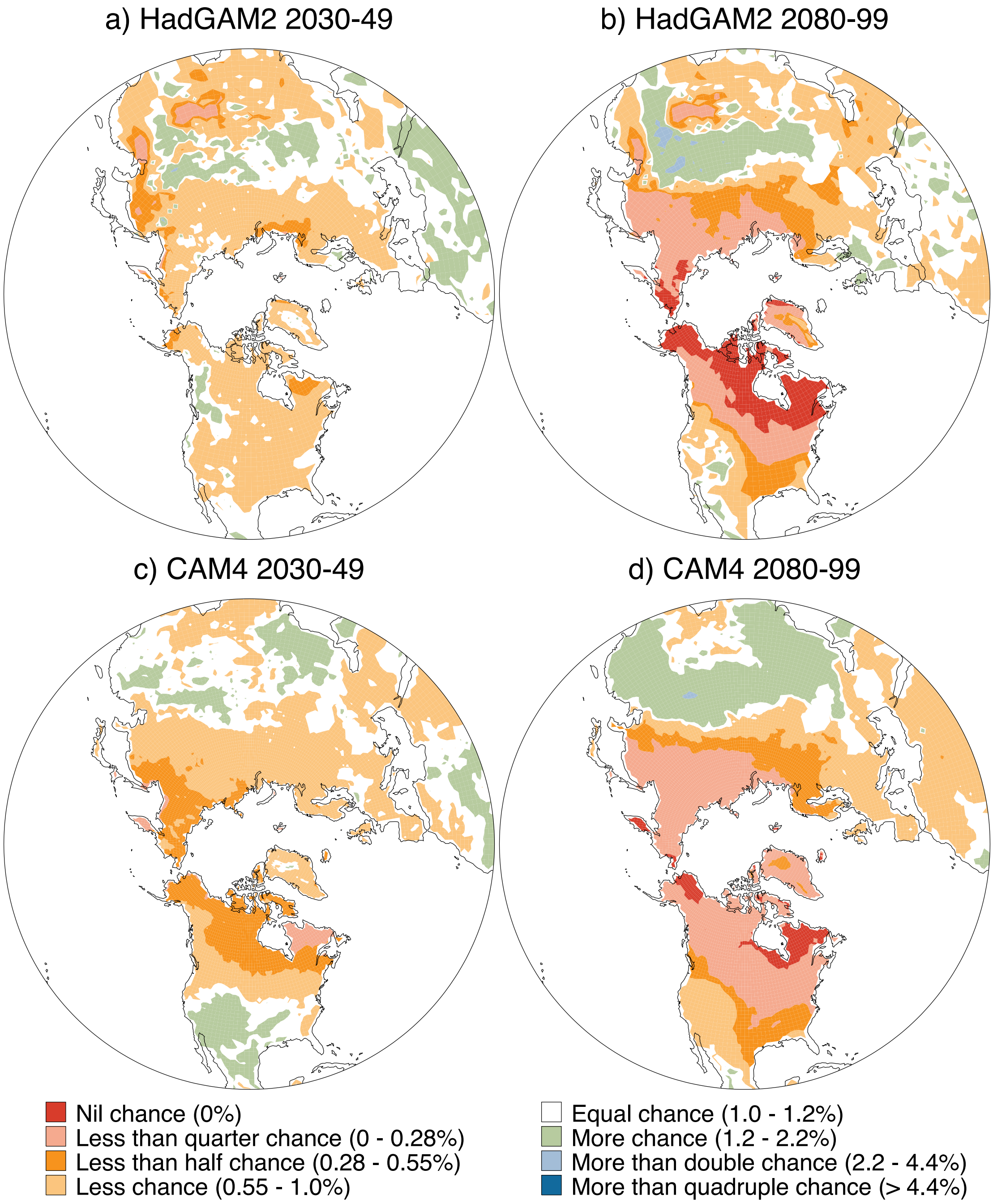

Figure 7. (**a**) Probability of extreme cold (defined as a winter daily temperature as cold or colder than the 1.1-percentile during the period 1980-99) in the sea ice forced HadGAM2 simulation for the period 2030-49. The colored shading categories are based on the relative change in probability compared to the period 1980-99. (**b**) As **a**, but for the period 2080-99 relative to 1980-99. (**c-d**) As **a-b**, but for the sea ice forced CAM4 simulations.

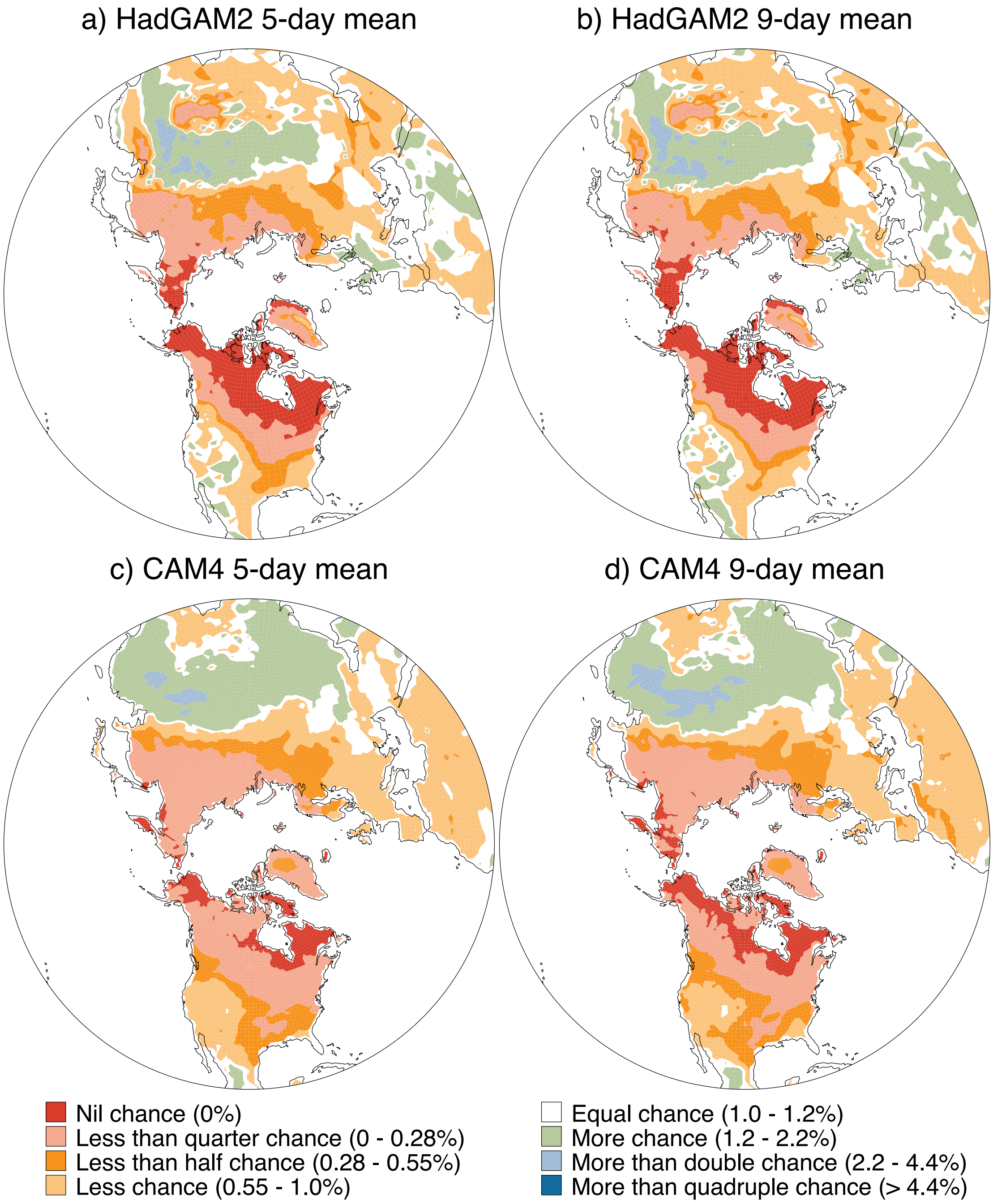

Figure 8. (**a**) Probability of extreme cold (defined as a winter 5-day mean temperature as cold or colder than the 1.1-percentile during the period 1980-99) in the sea ice forced HadGAM2 simulation for the period 2080-99. The colored shading categories are based on the relative change in probability compared to the period 1980-99. (**b**) As **a**, but for 9-day means. (**c-d**) As **a-b**, but for the sea ice forced CAM4 simulations.